AGU ADVANCING EARTH AND SPACE SCIENCE

Geophysical Research Letters®

RESEARCH LETTER
10.1029/2021GL097104

The 2021 South Sandwich Island M_w 8.2 Earthquake: A Slow Event Sandwiched Between Regular Ruptures

Zhe Jia[1], Zhongwen Zhan[1], and Hiroo Kanamori[1]

[1]Seismological Laboratory, California Institute of Technology, Pasadena, CA, USA

Key Points:

- The South Sandwich Island M_w 8.2 earthquake appears to have extended deep depth, yet displayed tsunami earthquake-like features
- Inversions including long-period data revealed a M_w 8.16 slow subevent at shallow depth, connecting regular deep ruptures at the ends
- The hybrid of deep and shallow ruptures represents an extreme example of the broad spectral behaviors of subduction zone earthquakes

Supporting Information:

Supporting Information may be found in the online version of this article.

Correspondence to:

Z. Jia,
zjia@gps.caltech.edu

Citation:

Jia, Z., Zhan, Z., & Kanamori, H. (2022). The 2021 South Sandwich Island M_w 8.2 earthquake: A slow event sandwiched between regular ruptures. *Geophysical Research Letters*, *49*, e2021GL097104. https://doi.org/10.1029/2021GL097104

Received 22 NOV 2021
Accepted 12 JAN 2022

Author Contributions:

Conceptualization: Zhe Jia, Zhongwen Zhan
Data curation: Zhe Jia
Formal analysis: Zhe Jia
Funding acquisition: Zhongwen Zhan
Investigation: Zhe Jia, Zhongwen Zhan, Hiroo Kanamori
Methodology: Zhe Jia
Project Administration: Zhe Jia
Resources: Zhe Jia, Hiroo Kanamori
Software: Zhe Jia, Hiroo Kanamori
Supervision: Zhe Jia, Zhongwen Zhan, Hiroo Kanamori
Validation: Zhe Jia
Visualization: Zhe Jia
Writing – original draft: Zhe Jia
Writing – review & editing: Zhe Jia, Zhongwen Zhan, Hiroo Kanamori

Abstract We determined the rupture sequence of the 12 August 2021 M_w 8.2 South Sandwich Island earthquake which appears to be a complex sequence in both time and space. Notable tsunamis were recorded by tide gauges at global distances. Given the complexity of this event, we conducted a multiple subevent inversion on broadband seismograms, to resolve its complex variations of fault geometry, location, depth, and temporal characteristics. We found that the rupture initiated as a regular deep thrust earthquake; it then ruptured shallower and triggered a silent and dominantly slow subevent extending ~200 km to the south, and ended with two other regular subevents. The total duration is ~260 s, unusually long for an M_w 8.2 event. Our result is qualitatively consistent with other moment tensor solutions and the deviant m_B–M_w and M_S–M_w relations, and provides a more quantitative space-temporal pattern of this unusual sequence.

Plain Language Summary The 2021 August South Sandwich Island M_w 8.2 earthquake was a surprise, because it was initially reported as a magnitude 7.5 event at a deep depth (47 km) but generated a global-spreading tsunami that would only be expected for a larger and shallower event. By using seismic data with period as long as 500 s, we revealed a hidden M_w 8.16 shallow slow event that happened between clusters of regular ruptures in the beginning and end. Although the slow event contributed 70% of the seismic moment, lasted three minutes, and ruptured a 200-km section of the plate interface, it is essentially invisible at short or intermediate periods, which explains its anomalously low body-wave and surface-wave magnitudes. The 2021 South Sandwich Island earthquake represents an extreme example of the broad spectral behaviors of subduction zone earthquakes and calls for attention in the research and warning of similar events.

1. Introduction

Large megathrust earthquakes on the subduction interface extend from near-trench to depths and display very different depth-varying slip behaviors (Lay et al., 2012). Large earthquakes that rupture the shallowest portion of the subduction interface (<15 km) can generate devastating tsunamis, but they appear to rupture slowly with inefficient excitation of short-period seismic waves disproportionately to their seismic moment and tsunami. These earthquakes are "tsunami earthquakes" (Kanamori, 1972). At deeper depths (15–50 km), large thrust earthquakes have faster rupture velocities and stronger radiation of short-period seismic energy with inefficient tsunami generation. Their contrasting rupture characteristics are well interpreted by two distinct types of fault properties; the slow slip of shallow tsunami earthquakes is commonly attributed to weak sediments and low rigidity of the upper plate (Bilek & Lay, 1999; Prada et al., 2021; Sallarès & Ranero, 2019), while the brittle failures of unstable fault patches explain the fast deeper earthquakes.

On 12 August 2021, a great earthquake (M_w > 8) struck the South Sandwich Island region of the south Atlantic Ocean (Figure 1a). This event occurred close to the South Sandwich trench, where the South American plate subducts beneath the South Sandwich plate at a velocity of 7 cm/year (Pelayo & Wiens, 1989). A remarkable observation of this earthquake is its far reaching-tsunamis. The tsunamis spread to the north Atlantic, Pacific, and Indian Oceans, where tide gauges measured peak amplitudes of ~20 cm at over 10,000 km distance from the source (Figure S1 in Supporting Information S1). Although modeling these tide gauge observations is challenging because of the lack of detailed bathymetry data between the source and gauges, the observed tsunamis at global distances appear to suggest that the South Sandwich Island earthquake could be categorized as a regular shallow tsunamigenic earthquake.

However, the South Sandwich Island earthquake seems to have extended to large depths with a complex temporal history. The early report (PDE) from the National Earthquake Information Center (NEIC) of the US Geological Survey listed two events within 3 min: (a) NEIC1, At 18:32:52 (UTC; 25.03°W, 57.68°S, Depth = 47.2 km,

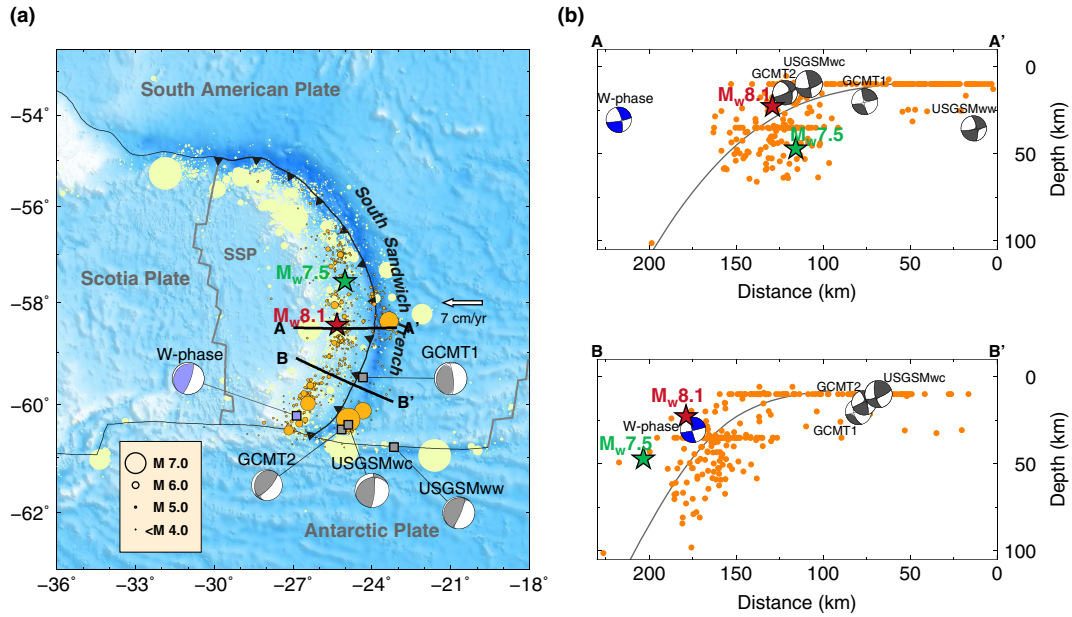

Figure 1. Overview of the tectonic setting and seismicity. (a) Tectonics of the South Sandwich region. The M_w 7.5 foreshock (green star) and the M_w 8.1 mainshock (red star) occurred close to the South Sandwich Trench, where the South America Plate subducts under the South Sandwich Plate. Yellow circles show the background seismicity according to the ISC catalog. Orange circles indicate the aftershocks within 2 weeks of the South Sandwich event. The beachballs display our W-phase moment tensor (in blue), USGS NEIC M_{wc}, M_{ww}, and two Global CMT solutions (in gray). (b) Cross-sections along the black line segments in (a). The orange dots indicate the aftershocks within 100 km of the profiles. The black line represents the Slab 2.0 interface. Beachballs and stars are the same as (a), but for side view.

M_w = 7.5) and (b) NEIC2, At 18:35:17 (25.26°W, 58.38°S, Depth = 22.8 km, M_w = 8.1). In this paper, we call collectively the earthquake sequence which started at 18:32:52 (UTC) and lasted for about 300 s, the 2021 South Sandwich Island earthquake, and we refer the first (NEIC1) and second (NEIC2) events as the foreshock and the mainshock, respectively. The Global Centroid Moment Tensor Project (GCMT) (Ekström et al., 2012) reported two events: (a) GCMT1 (202108121832A, centroid time: 18:35:25, M_w = 8.3, 24.34°W, 59.48°S, depth = 20.0 km) and (b) GCMT2 (202108121835A, centroid time: 18:36:13, M_w = 7.9, 25.15°W, 60.47°S, depth = 15.1 km). USGS NEIC also reported a moment tensor solution at the centroid time around 18:36 with M_{wc} = 7.98 and depth = 10 km with an alternative solution with M_{ww} = 8.13 and depth = 35.5 km (more details in Table S1 in Supporting Information S1). Given the variability of these solutions, we attempted W-phase inversion (Kanamori and Rivera, 2008). Because of the complex interference of the waveforms of several events, only with a very narrow long-period pass band (0.00125–0.002 Hz, i.e., 500–800 s), we could obtain a solution that can fit long-period waveforms satisfactorily for 40 stations (more details in Text S1, Figures S2 and S3 in Supporting Information S1).

The depths reported by different catalogs range from 10 to 50 km, and the hypocenters scatter around the Slab 2.0 (Hayes et al., 2018) interface (Figure 1b). This is probably caused by difficulty in locating the events accurately, due to the complex interference of seismic waves from the foreshock and mainshock. Nevertheless, the deeper depths of the South Sandwich Island earthquake appear to contradict the shallow slip inferred from the global-spreading tsunami. While detailed rupture analyses would be needed to understand this disparity, it is difficult to define a physical fault plane for slip inversions due to the diverse locations and focal mechanisms from different sources (Figure 1). In addition, the aftershocks extend ~400 km along the curved subduction zone, making a planar fault unphysical. Thus, we need to analyze the rupture properties of this earthquake with flexibility in fault geometries, while maintaining the depth-dependent complexities.

In this study, we first investigate the overall spectral characteristics of the event. Then, we determine the kinematic rupture process with a multiple subevent inversion of broad-band seismic waveforms, and evaluate the contributions of subevents and discuss their relationships.

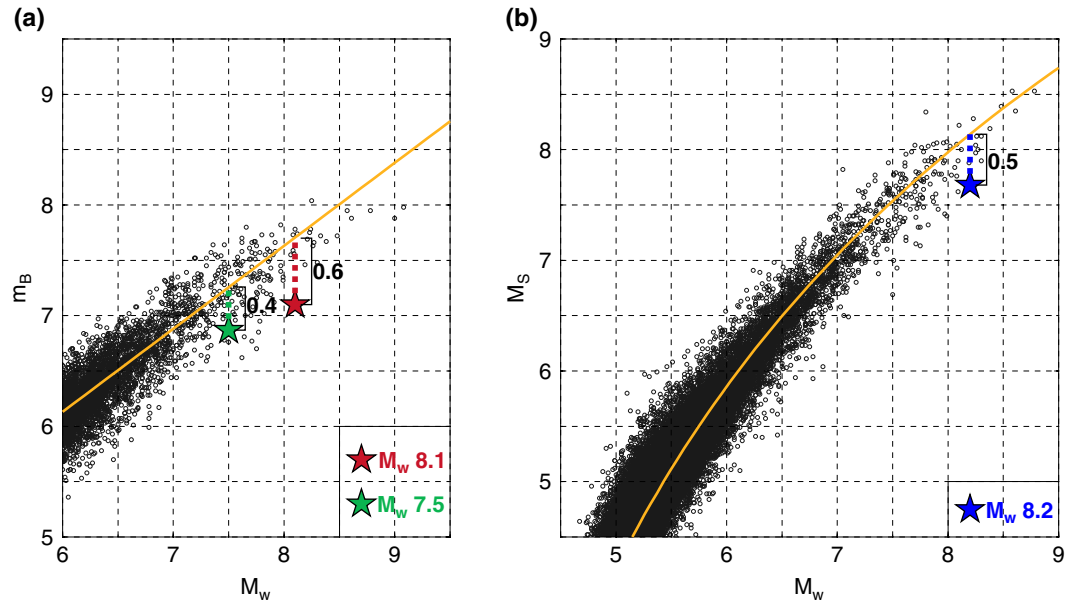

Figure 2. m_B and M_S measurements for the South Sandwich Island sequence. (a) Body wave magnitude m_B for the M_w 7.5 foreshock (green star) and the M_w 8.1 mainshock (red star). The solid yellow line indicates the general trend, $m_B = 0.75 M_w + 1.63$ (Kanamori & Ross, 2019), which is regressed from the database of global earthquakes for the period 1988–2018 (black circles). (b) Surface wave magnitude M_S for the sequence. The solid yellow line shows the empirical relation, $M_w = \exp(-0.222 + 0.233 M_S) + 2.863$, regressed from the historical earthquakes (black circles) in the GCMT catalog (Di Giacomo et al., 2015).

2. General Spectral Characteristics

Given the complex rupture characteristics of the 2021 South Sandwich Island earthquake, we first investigate this event using three magnitude scales, m_B, M_S, and M_w. Although m_B and M_S are old somewhat qualitative parameters, they are available for global earthquakes and useful for understanding the spectral characteristics of the South Sandwich Island sequence in global context. To the first order, m_B, M_S, and M_w represent the spectral amplitudes of the sequence at about 4, 20, and 200 s or even longer period.

2.1. m_B Versus M_w Relationship

For the measurement of m_B, we used the method described in Kanamori and Ross (2019) which follows the method developed by Gutenberg and Richter (1956). We used the vertical component P-waves recorded at 54 global network stations (epicentral distance of 30°–80°, Figure S4 in Supporting Information S1), which include peak amplitudes for the mainshock. The medians of station m_B are 6.87 and 7.10 for the foreshock and the mainshock, respectively. Figure 2a compares the m_B–M_w relationship for these events with the m_B values of about 3,000 events with $M_w \geq 6$ for a period from 1988 to 2018 taken from Kanamori and Ross (2019). The m_B data for the global events shown by small dots represent the range for ensemble of global events. The m_B for the mainshock is probably the upper bound because the time window for the m_B measurements contains some energy from the foreshock, only 145 s earlier. The m_B values for the foreshock and the mainshock are 0.4 and 0.6 m_B unit, respectively, smaller than the average global m_B–M_w trend; this indicates that these events, especially the mainshock, are deficient in short-period energy.

2.2. M_S Versus M_w Relationship

We made a similar comparison of M_S versus M_w relationship. We computed M_S using 20 s surface waves from 483 global seismic stations (distance range of 30°–120°), and measured the peak ground motion amplitudes. Since the surface waves of the foreshock and mainshock overlap, we could not measure M_S for each event separately, and obtained just one $M_S = 7.68$ (Figure S5 in Supporting Information S1). Compared with the empirical global

M_S–M_w relationship (Di Giacomo et al., 2015) from the ISC M_S data set (ISC, 2021), the observed M_S is 0.5 smaller than the average trend (Figure 2b).

The smaller m_B and M_S than the global average trends indicate depleted seismic energy release at short periods and slow rupturing characteristics (Kanamori, 1972; Kanamori & Ross, 2019). As shown in Figures 2a and 2b, the South Sandwich Island earthquake is among the biggest outliers from the general trend. Other anomalous events similar to the South Sandwich Island earthquake includes the 1992 Nicaragua M_w 7.6, the 1994 Java M_w 7.8, the1996 Peru M_w 7.5, the 2006 M_w 7.7 Java, and the 2010 M_w 7.8 Mentawai Island earthquakes, all of which are well-known shallow slow tsunami earthquakes. This similarity suggests that the South Sandwich Island earthquake probably involved a substantial slow rupture component at the shallow subduction interface.

3. Multiple Subevent Inversion

To image the detailed rupture process of the earthquake, we applied the multiple subevent inversion method. Our subevent inversion algorithm represents a complex rupture with multiple simpler sources, each of which can have different timings, locations, source durations and focal mechanisms (Jia, Shen, et al., 2020; Jia, Wang, & Zhan, 2020; Ross et al., 2019; Zhan et al., 2014). This simple parameterization allows flexible representation of time history and fault geometries, thereby capturing the first-order spatiotemporal rupture complexities. Our subevent method is particularly suitable for describing the South Sandwich Island earthquake which contains at least two major events in 3 min and involves potential fault geometry variations along the curved South Sandwich trench. As the possible slow rupture may propagate long distance with strong directivity effects, we introduce a finite subevent with a unilateral Haskell rupture model with a constant rupture velocity (Haskell, 1964). In this study, we use the Haskell model only for the long duration (>100 s) subevent with potentially significant rupture directivity. We applied a Markov Chain Monte Carlo inversion in a Bayesian framework, and increased the number of subevents iteratively until the waveforms fit well (Text S2 in Supporting Information S1 for more details).

We collected 58 teleseismic (distance of 30°–90°) P velocity and displacement records, 43 teleseismic SH displacement records, and 12 three-component regional (distance within 40°) full waveforms in displacement (Figure S6 in Supporting Information S1) for the subevent inversion. We removed their instrumental responses, and filtered the P and SH waves between 0.005 and 0.05 Hz for modeling short period features. For the regional full waves, we used them in two datasets with different filter bands. One of them with a 0.002–0.02 Hz passband represents intermediate period waves, and the other with 0.002–0.0033 Hz, long period motions. This combination of short, intermediate and long period bands allows mapping the ruptures of different length scales simultaneously. The teleseismic Green's functions are calculated combining the propagator matrix method and plane wave approximation (Kikuchi & Kanamori, 1991; Qian et al., 2017), using the CRUST 2.0 (Laske et al., 2001) model at the source region and the IASPEI91 model (Kennet, 1991) at other places. The regional full-wave synthetics are computed with a frequency-wavenumber integration algorithm (Zhu & Rivera, 2002), using the PREM model (Dziewonski & Anderson, 1981).

Our subevent model consists of five subevents that span ~300 km along the trench (Figure 3, Table S2 in Supporting Information S1). We fixed the first subevent at the NEIC M_w 7.5 event hypocenter. Data fittings (Figure 3c, Figure S7 in Supporting Information S1) and model uncertainties (Figure 3b, Figure S8 in Supporting Information S1) suggest that the source parameters are well constrained. The rupture begins with two short-duration subevents E1 (centroid time $\tau_C = 13$s after the origin time, duration $d_C = 23$s, M_w 7.2) and E2 ($\tau_C = 36$s, $d_C = 19$s, M_w 7.2), which in total (M_w 7.4) generally represents the NEIC M_w 7.5 foreshock. They have close locations and similar shallow dipping thrust focal mechanisms (average strike/dip/rake = 157°/18°/82°), but the centroid depth of E1 is deep (39 km) while E2 is shallow (7 km), suggesting an updip rupture propagation along the plate interface. They are located near a patch of dense aftershock seismicity (Figure 3a).

Concurrent with the rupture initiation represented by E1–E2 in the first 50 s, the subevent E3 ($\tau_C = 90$s, M_w 8.16) emerged and continued for ~180 s. E3 contributes the most seismic moment of the South Sandwich Island earthquake, and its moment rate function (Figure 3d) has a remarkably smaller aspect ratio (peak moment rate over duration, 1.2×10^{17} N-m/s^2) than regular subevents E1–E2 (average of 3.3×10^{17} N-m/s^2). As a Haskell source, E3 initiates close to the locations of E1–E2, and unilaterally propagates toward the south with a slow velocity (~1 km/s) and a long fault length (~180 km). E3 is located at 14 km depth with an uncertainty of ±5 km (Figure 3b), and it has a very shallow-dipping thrust mechanism (strike/dip/rake = 134°/4°/22°), although the strike

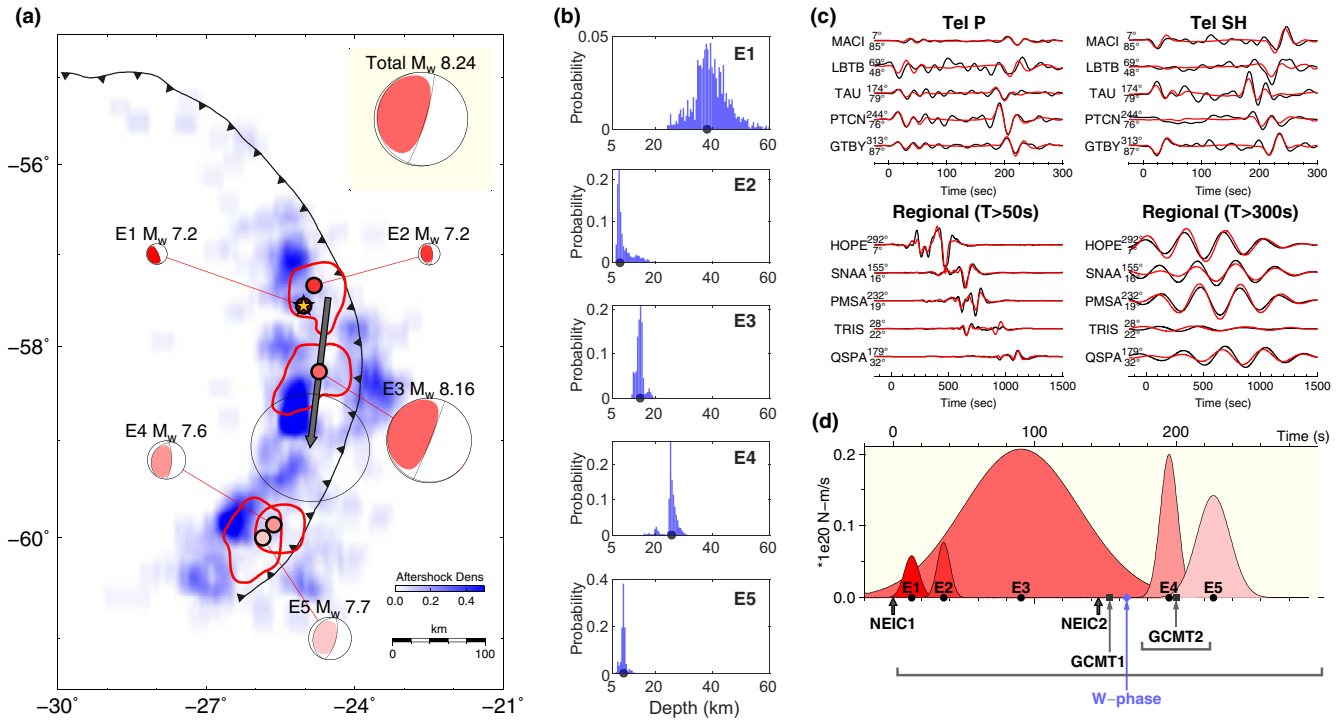

Figure 3. Rupture process of the South Sandwich Island sequence. (a) Subevent locations (red dots) and focal mechanisms (red beachballs). Yellow star indicates the hypocenter, collocated with the first subevent E1. The red contours show 95% confidence limits of the subevent locations. The gray arrow at E3 indicates its rupture directivity, and its length reflects rupture length. The black contour at the arrow end shows the 95% confidence limit of the rupture length and direction of E3, assuming the back end as the starting point. The aftershock density is displayed by the blue background color. The inset box shows the summation of subevent moment tensors. (b) Marginal probability distributions of subevent centroid depths. Gray circles show the final depths. (c) Representative data (black) and synthetic (red) waveform fits for teleseismic P and SH waves (0.005–0.05 Hz), vertical component intermediate period (0.002–0.02 Hz) and long period regional (0.002–0.0033 Hz) full waves. The numbers leading the traces are azimuths and distances. (d) Moment rate functions for all subevents. The black circles indicate subevent centroid times. The dark arrows point to two NEIC event origin times. Gray squares and blue diamonds indicate centroid times of the GCMT and W-phase solutions, and the underneath solid lines denote the corresponding source durations.

and rake angles are not well constrained due to the shallow dip angle (Figure S9 in Supporting Information S1). The shallow slow slip of E3 presumably transfers the stress along the slab, which explains the downdip dense aftershock seismicity as well as the triggered outer-rise earthquakes (Figure 3).

The rupture terminated with the final two subevents E4 (τ_C = 195s, d_C = 26s, M_w 7.6) and E5 (τ_C = 226s, d_C = 50s, M_w 7.7) at 250–300 km south of the epicenter. They occurred about 3 min after the rupture initiation. E4 and E5 are also shallow dipping thrust subevents (average strike/dip/rake = 206°/23°/106°), but their strike angles are ~50° rotated clockwise from E1–E2. This rotation is consistent with the geometry of the curved South Sandwich Island trench. Their locations are close to the downdip high-density aftershock patch (Figure 3). This spatial pattern is similar to that for the other two major slip asperities (E1–E2 and E3). The depth of E4 (25 km) is significantly deeper than E5 (9 km), indicating coexisting megathrust slip at different depth domains. Moment rate functions of E4-E5 display similar aspect ratios (average of 5.3×10^{17} N-m/s^2) to E1–E2, indicating that E4 and E5 are, unlike E3, more like regular ruptures.

The low aspect ratio, slow rupture velocity, overall shallow depth, and shallow-dipping mechanism of E3 suggest that it is a "slow earthquake" at the shallow subduction interface. This feature can be most prominently demonstrated in Figure 4. The regular subevents E1, E2, E4, and E5 contributed almost all of the short and intermediate period waveforms, while E3 barely excited short and intermediate period signals (Figures 4a–4c and S10 in Supporting Information S1). In contrast, E3 generated large long-period waves, comparable to the sum of all other subevents (Figure 4d, Figure S10 in Supporting Information S1). The diminished short period excitation explains the smaller-than-average m_B and M_S of E3 (Figure 2).

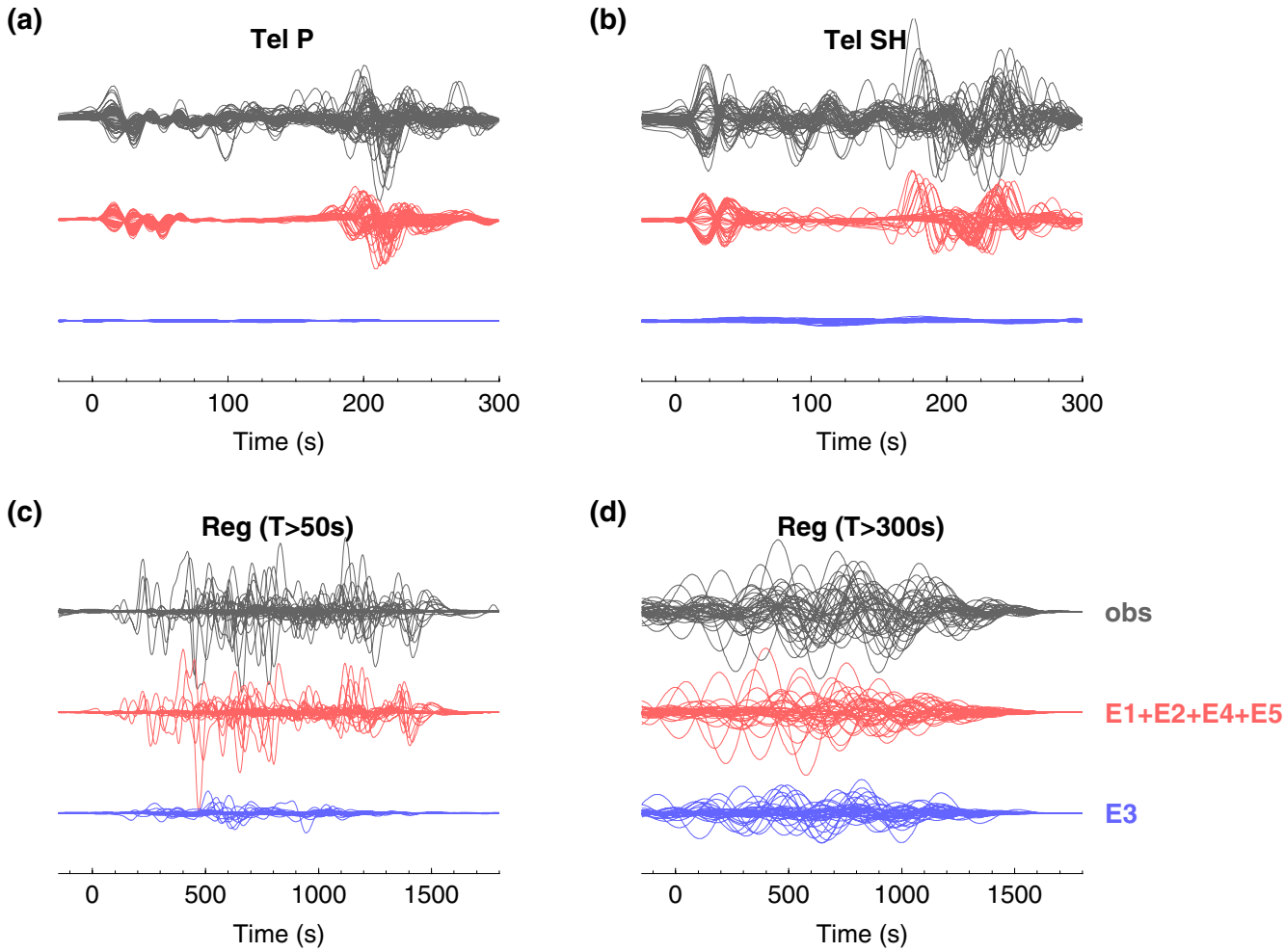

Figure 4. Waveform contributions from two groups of subevents. The observed data for all stations are plotted together in black lines. The total contribution from regular subevents E1, E2, E4, E5 are in red lines. The synthetics of the slow subevent E3 are indicated by blue lines. (a) P waves. (b) SH waves. (c) Intermediate period (0.002–0.02 Hz) and (d) long period (0.002–0.0033 Hz) regional full waveforms.

Figure 3d compares the overall rupture sequence determined by our multiple subevent inversion with the events determined by other methods. The sequence starts with E1 which is the foreshock (NEIC1). The long duration subevent E3 connects the short duration subevents E1–E2 at the beginning and E4–E5 at the end, forming a continuous megathrust rupture process. This approximately corresponds to the unusually long-duration GCMT1 (M_w 8.3) in the middle of the rupture extent (Figure 1). The GCMT2 (M_w 7.9, half duration = 24 s), with the centroid time 48 s later than GCMT1 probably overlaps with GCMT1 in time, and roughly corresponds to E4-E5 at the southern tip with rotated strike angles (Figure 1). The W-phase solution, which is similar to the NEIC M_{ww}, probably represents a very long-period component of the latter half of the sequence (Figure 1, Figure S2 in Supporting Information S1).

4. Discussion and Conclusions

The 2021 South Sandwich Island (M_w 8.2) earthquake is a complex multiple event, including a slow subevent E3 connecting other regular thrust subevents at the beginning and the end. The slow subevent E3 contributes over 70% of the total seismic moment of the sequence. The large moment and the relatively shallow depth of E3, with weak short-period seismic radiation, make this sequence as a whole look like a tsunami earthquake. The total duration of the whole sequence (E1 to E5) is about 260 s; thus, the centroid time shift, 130 s, estimated from the half duration is anomalously long on the centroid time delay versus M_w scaling relation obtained by Duputel et al. (2013), as shown by Figure 5. The 2002 Guerrero earthquake (Kostoglodov et al., 2003) and the 2006 Java

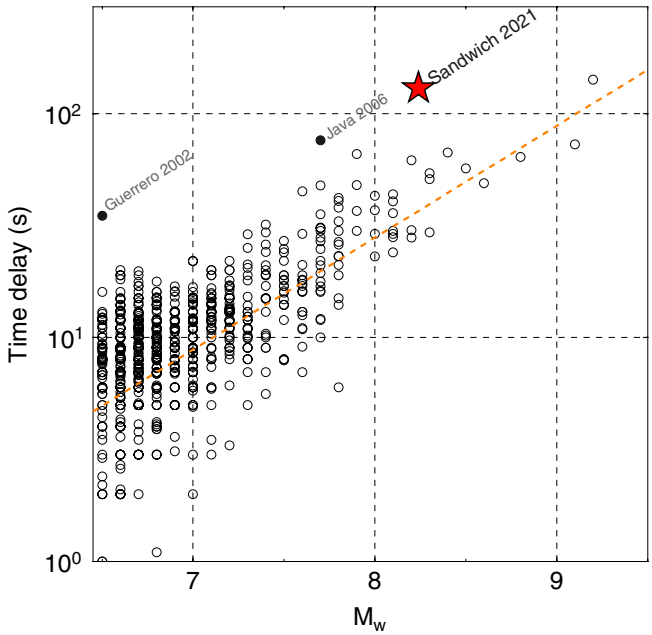

Figure 5. Relation between time delay (half duration) and M_w for the South Sandwich Island event (red star). Black circles represent the time delays of historical events from the W-phase measurements, the orange dashed line indicates an exponential relationship using the stress parameter of 0.37 MPa (Duputel et al., 2013).

earthquake (Ammon et al., 2006), both of which are slow tsunami earthquakes, share a similar trend on Figure 5. Thus, the South Sandwich Island earthquake appears to be a hybrid of deep rupture and slow tsunamigenic slip; this explains the somewhat unusual combination of the relatively large depth and the globally observed tsunami.

Although the shallowest subduction interface is often considered seismically inactive due to the velocity-strengthening frictional properties (Scholz, 1998), some large tsunami earthquakes were found to host major slip at near-trench depths (Kanamori & Kikuchi, 1993; Lay et al., 2011). Lower upper plate rock rigidity at shallow depths has been illustrated to produce tsunami earthquake-like properties, including depleted short period seismic energy and slow rupture (Bilek & Lay, 1999; Sallarès & Ranero, 2019; Sallares et al., 2021), which well explains our observations for E3, suggesting the subduction zone geologic conditions could largely impact the tsunami potential. However, the slow component of the South Sandwich Island earthquake may have a broader depth extent than the traditional tsunami earthquakes. The slow subevent E3 has an overall shallow centroid depth of 14 km, which explains its global-spreading tsunamis and the two large (~M_w 7) outer-rise aftershocks (Figure 1) due to the possible stress transfer at shallow subduction interface (Sladen & Trevisan, 2018). However, it is probably not confined in the near-trench depths like other tsunami earthquakes, but could have extended to deeper domains, which is consistent with absence of observation of devastating tsunami. The deeper slip could trigger slow rupture by dynamic weakening (Ma, 2012; Noda & Lapusta, 2013), making the slip span over a broad depth range. However, the detailed depth-dependent slip distribution of the slow subevent remains unclear and difficult to resolve, because of the tradeoff between seismic moment, dip angle and depth (Tsai et al., 2011). This requires further investigations.

In summary, the 2021 South Sandwich Island M_w 8.2 earthquake involves a complex depth-varying rupture process. The complex interaction of deep regular slip and shallow slow subevent explains the somewhat contradicting combination of the deep subevents, the tsunami earthquake-like features with diminished short-period seismic radiation and the global-spreading tsunamis. This highlights the importance of accurately mapping the slow components of megathrust earthquakes over a broad frequency band for reliable tsunami warning.

Data Availability Statement

All figures are plotted using GMT (https://www.generic-mapping-tools.org/) and MATLAB (http://www.mathworks.com/) software. Seismic data are available on the IRIS Wilber 3 page (https://ds.iris.edu/wilber3/find_stations/11455082). Tide gauge data are available on the IOC sea level page (http://www.ioc-sealevelmonitoring.org/list.php).

Acknowledgments
We thank the IRIS for providing public access (http://ds.iris.edu/wilber3/find_event) to all the seismic data. We thank the IOC of UNESCO for providing public access (http://www.ioc-sealevelmonitoring.org/) to the tide gauge data. We thank Luis Rivera and Gregory Beroza for constructive discussions, and thank two anonymous reviewers for their comments. This work is supported by USGS grant G19AP00030.

References

Ammon, C. J., Kanamori, H., Lay, T., & Velasco, A. A. (2006). The 17 July 2006 Java tsunami earthquake. *Geophysical Research Letters*, *33*(24), L24308. https://doi.org/10.1029/2006gl028005

Bilek, S. L., & Lay, T. (1999). Rigidity variations with depth along interplate megathrust faults in subduction zones. *Nature*, *400*(6743), 443–446. https://doi.org/10.1038/22739

Di Giacomo, D., Bondár, I., Storchak, D. A., Engdahl, E. R., Bormann, P., & Harris, J. (2015). ISC-GEM: Global Instrumental Earthquake Catalogue (1900–2009), III. Re-computed MS and mb, proxy MW, final magnitude composition and completeness assessment. *Physics of the Earth and Planetary Interiors*, *239*, 33–47. https://doi.org/10.1016/j.pepi.2014.06.005

Duputel, Z., Tsai, V. C., Rivera, L., & Kanamori, H. (2013). Using centroid time-delays to characterize source durations and identify earthquakes with unique characteristics. *Earth and Planetary Science Letters*, *374*, 92–100. https://doi.org/10.1016/j.epsl.2013.05.024

Dziewonski, A. M., & Anderson, D. L. (1981). Preliminary reference Earth model. *Physics of the Earth and Planetary Interiors*, *25*(4), 297–356. https://doi.org/10.1016/0031-9201(81)90046-7

Ekström, G., Nettles, M., & Dziewoński, A. (2012). The global CMT project 2004–2010: Centroid-moment tensors for 13,017 earthquakes. *Physics of the Earth and Planetary Interiors*, *200*, 1–9.

Gutenberg, B., & Richter, C. F. (1956). Earthquake magnitude, intensity, energy, and acceleration: (Second paper). *Bulletin of the Seismological Society of America*, *46*(2), 105–145. https://doi.org/10.1785/bssa0460020105

Haskell, N. (1964). Total energy and energy spectral density of elastic wave radiation from propagating faults. *Bulletin of the Seismological Society of America*, *54*(6A), 1811–1841. https://doi.org/10.1785/bssa05406a1811

Hayes, G. P., Moore, G. L., Portner, D. E., Hearne, M., Flamme, H., Furtney, M., & Smoczyk, G. M. (2018). Slab2, a comprehensive subduction zone geometry model. *Science*, *362*(6410), 58–61. https://doi.org/10.1126/science.aat4723

International Seismological Centre. (2021). The ISC MS dataset for shallow earthquakes since 1904. *ISC Seismological Dataset Repository*. https://doi.org/10.31905/0N4HOS2D

Jia, Z., Shen, Z., Zhan, Z., Li, C., Peng, Z., & Gurnis, M. (2020). The 2018 Fiji Mw8.2 and 7.9 deep earthquakes: One doublet in two slabs. *Earth and Planetary Science Letters*, *531*, 115997. https://doi.org/10.1016/j.epsl.2019.115997

Jia, Z., Wang, X., & Zhan, Z. (2020). Multifault models of the 2019 ridgecrest sequence highlight complementary slip and fault junction instability. *Geophysical Research Letters*, *47*(17), e2020GL089802. https://doi.org/10.1029/2020gl089802

Kanamori, H. (1972). Mechanism of tsunami earthquakes. *Physics of the Earth and Planetary Interiors*, *6*(5), 346–359. https://doi.org/10.1016/0031-9201(72)90058-1

Kanamori, H., & Kikuchi, M. (1993). The 1992 Nicaragua earthquake: A slow tsunami earthquake associated with subducted sediments. *Nature*, *361*(6414), 714–716. https://doi.org/10.1038/361714a0

Kanamori, H., & Rivera, L. (2008). Source inversion ofWphase: Speeding up seismic tsunami warning. *Geophysical Journal International*, *175*(1), 222–238. https://doi.org/10.1111/j.1365-246x.2008.03887.x

Kanamori, H., & Ross, Z. E. (2019). Reviving m B. *Geophysical Journal International*, *216*(3), 1798–1816. https://doi.org/10.1093/gji/ggy510

Kennet, B. (1991). IASPEI 1991 seismological tables. *Terra Nova*, *3*(2), 122. https://doi.org/10.1111/j.1365-3121.1991.tb00863.x

Kikuchi, M., & Kanamori, H. (1991). Inversion of complex body waves—III. *Bulletin of the Seismological Society of America*, *81*(6), 2335–2350. https://doi.org/10.1785/bssa0810062335

Kostoglodov, V., Singh, S. K., Santiago, J. A., Franco, S. I., Larson, K. M., Lowry, A. R., & Bilham, R. (2003). A large silent earthquake in the Guerrero seismic gap, Mexico. *Geophysical Research Letters*, *30*(15), 1807. https://doi.org/10.1029/2003gl017219

Laske, G., Masters, G., & Reif, C. (2001). *CRUST 2.0: A new global crustal model at 2 × 2 degrees*. Institute of Geophysics and Planetary Physics The University of California. Retrieved from http://mahi.ucsd.edu/Gabi/rem.dir/crust/crust2.html

Lay, T., Ammon, C. J., Kanamori, H., Yamazaki, Y., Cheung, K. F., & Hutko, A. R. (2011). The 25 October 2010 Mentawai tsunami earthquake (Mw7.8) and the tsunami hazard presented by shallow megathrust ruptures. *Geophysical Research Letters*, *38*, L06302. https://doi.org/10.1029/2010gl046552

Lay, T., Kanamori, H., Ammon, C. J., Koper, K. D., Hutko, A. R., Ye, L., et al. (2012). Depth-varying rupture properties of subduction zone megathrust faults. *Journal of Geophysical Research*, *117*, B04311. https://doi.org/10.1029/2011jb009133

Ma, S. (2012). A self-consistent mechanism for slow dynamic deformation and tsunami generation for earthquakes in the shallow subduction zone. *Geophysical Research Letters*, *39*, L11310. https://doi.org/10.1029/2012gl051854

Noda, H., & Lapusta, N. (2013). Stable creeping fault segments can become destructive as a result of dynamic weakening. *Nature*, *493*(7433), 518–521. https://doi.org/10.1038/nature11703

Pelayo, A. M., & Wiens, D. A. (1989). Seismotectonics and relative plate motions in the Scotia Sea region. *Journal of Geophysical Research: Solid Earth*, *94*(B6), 7293–7320. https://doi.org/10.1029/jb094ib06p07293

Prada, M., Galvez, P., Ampuero, J., Sallares, V., Sánchez-Linares, C., Macías, J., & Peter, D. (2021). The influence of depth-varying elastic properties of the upper plate on megathrust earthquake rupture dynamics and tsunamigenesis. *Journal of Geophysical Research: Solid Earth*, *126*. https://doi.org/10.1029/2021jb022328

Qian, Y., Ni, S., Wei, S., Almeida, R., & Zhang, H. (2017). The effects of core-reflected waves on finite fault inversions with teleseismic body wave data. *Geophysical Journal International*, *211*(2), 958–973. https://doi.org/10.1093/gji/ggx338

Ross, Z. E., Idini, B., Jia, Z., Stephenson, O. L., Zhong, M., Wang, X., et al. (2019). Hierarchical interlocked orthogonal faulting in the 2019 Ridgecrest earthquake sequence. *Science*, *366*(6463), 346–351. https://doi.org/10.1126/science.aaz0109

Sallarès, V., Prada, M., Riquelme, S., Meléndez, A., Calahorrano, A., Grevemeyer, I., & Ranero, C. R. (2021). Large slip, long duration, and moderate shaking of the Nicaragua 1992 tsunami earthquake caused by low near-trench rock rigidity. *Science Advances*, *7*(32), eabg8659.

Sallarès, V., & Ranero, C. R. (2019). Upper-plate rigidity determines depth-varying rupture behaviour of megathrust earthquakes. *Nature*, *576*(7785), 96–101.

Scholz, C. H. (1998). Earthquakes and friction laws. *Nature*, *391*(6662), 37–42. https://doi.org/10.1038/34097

Sladen, A., & Trevisan, J. (2018). Shallow megathrust earthquake ruptures betrayed by their outer-trench aftershocks signature. *Earth and Planetary Science Letters*, *483*, 105–113. https://doi.org/10.1016/j.epsl.2017.12.006

Tsai, V. C., Hayes, G. P., & Duputel, Z. (2011). Constraints on the long-period moment-dip tradeoff for the Tohoku earthquake. *Geophysical Research Letters*, *38*(7). https://doi.org/10.1029/2011gl049129

Zhan, Z., Kanamori, H., Tsai, V. C., Helmberger, D. V., & Wei, S. (2014). Rupture complexity of the 1994 Bolivia and 2013 Sea of Okhotsk deep earthquakes. *Earth and Planetary Science Letters*, *385*, 89–96. https://doi.org/10.1016/j.epsl.2013.10.028

Zhu, L., & Rivera, L. A. (2002). A note on the dynamic and static displacements from a point source in multilayered media. *Geophysical Journal International*, *148*(3), 619–627. https://doi.org/10.1046/j.1365-246x.2002.01610.x